Role of Intertube Interactions in Double- and Triple-Walled Carbon Nanotubes

Thomas Ch. Hirschmann,[†,‡,*] Paulo T. Araujo,[‡,∞,*] Hiroyuki Muramatsu,[⊥] Joaquin F. Rodriguez-Nieva,[§] Max Seifert,[∥] Kornelius Nielsch,[†] Yoong Ahm Kim,[¶,#] and Mildred S. Dresselhaus[‡,§,*]

[†]Institute of Applied Physics, University of Hamburg, 20355 Hamburg, Germany, [‡]Department of Electrical Engineering and Computer Science, and [§]Department of Physics, Massachusetts Institute of Technology, Cambridge, Massachusetts 02139-4307, United States, [∞]Department of Physics and Astronomy, University of Alabama, Tuscaloosa, Alabama 35487, United States, [⊥]Department of Materials Science and Technology, Nagaoka University of Technology, 1603-1 Kamitomioka, Nagaoka 940-2188, Japan, [∥]Walter Schottky Institut and Physik Department, Technische Universität München, 85748 Garching, Germany, [¶]Faculty of Engineering, Shinshu University, 4-17-1 Wakasato, Nagano 380-8553, Japan, and [#]Polymer and Fiber System Engineering, Chonnam National University, 77 Yongbong-ro, buk-gu, Gwangju 500-757, Korea

ABSTRACT Resonant Raman spectroscopy studies are performed to access information about the intertube interactions and wall-to-wall distances in double- and triple-walled carbon nanotubes. Here, we explain how the surroundings of the nanotubes in a multiwalled system influence their radial breathing modes. Of particular interest, the innermost tubes in double- and triple-walled carbon nanotube systems are shown to be significantly shielded from environmental interactions, except for those coming from the intertube interaction with their own respective host tubes.

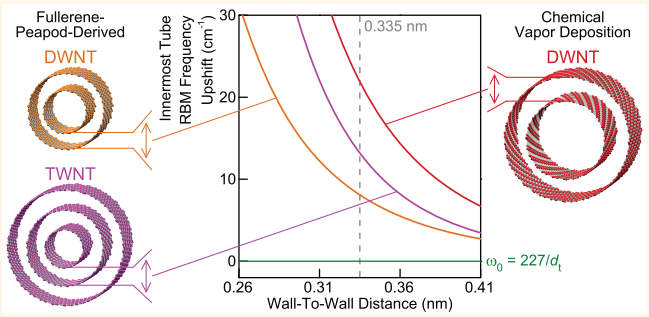

From a comparison of the Raman results for bundled as well as individual fullerene-peapod-derived double- and triple-walled carbon nanotubes, we observe that metallic innermost tubes, when compared to their semiconducting counterparts, clearly show weaker intertube interactions. Additionally, we discuss a correlation between the wall-to-wall distances and the frequency upshifts of the radial breathing modes observed for the innermost tubes in individual double- and triple-walled carbon nanotubes. All results allow us to contemplate fundamental properties related to DWNTs and TWNTs, as for example diameter- and chirality-dependent intertube interactions. We also discuss differences in fullerene-peapod-derived and chemical vapor deposition grown double- and triple-walled systems with the focus on mechanical coupling and interference effects.

KEYWORDS: double-walled carbon nanotubes · triple-walled carbon nanotubes · resonant Raman spectroscopy · radial breathing modes · intertube interactions · wall-to-wall distances

Various fabrication methods are used to produce double-walled carbon nanotubes (DWNTs). Among these methods, the catalytic chemical vapor deposition (CVD) process,[1] the arc-discharge process,[2] and the peapod-derived process[3] are best known and have been most widely discussed in the literature. Starting in 1998, the peapod growth method has by now become well-established.[4] According to this method, C_{60} carbon sources (fullerene peapods) are, for example, filled into a host single-walled carbon nanotube (SWNT) array with an average diameter of about 1.4 nm.[4] After high-temperature heat treatment of these aligned peapods, they form an additional coaxial innermost tube *via* a thermal energy mechanism and a DWNT is produced.[5] Some factors affect the peapod growth of the innermost tube, as for example the diameter distribution of the host tubes, the annealing time, the annealing temperature, and the carbon growth source (fullerenes,[6] ferrocenes,[7] anthracenes,[8] or graphene nanoribbons[9]). Recently, it has been shown that this peapod growth method for DWNTs also can be extended to produce high-quality triple-walled carbon nanotubes (TWNTs).[10] However, in this case, the host for the carbon source is a diameter-enlarged CVD-grown DWNT instead of a SWNT.

Resonant Raman spectroscopy (RRS) provides a powerful tool to characterize and understand carbon nanotubes and reveals an abundance of information about both the growth method and the quality of nanotube that is produced.[11] The most important and unique Raman signature of carbon

* Address correspondence to thirschm@physnet.uni-hamburg.de, paulo.t.araujo@ua.edu, millie@mgm.mit.edu.

Received for review September 15, 2013 and accepted January 23, 2014.

Published online January 23, 2014
10.1021/nn500420s

nanotubes is the coherent breathing of the carbon atoms normal to the tube circumference: the so-called radial breathing mode (RBM). The RBM frequency (ω_{RBM}) allows us to access a multitude of information about the nanotube properties because ω_{RBM} is inversely proportional to the carbon nanotube diameter (d_t), which is known to be a function of the nanotube (n,m) indices.[11] As a matter of fact, the knowledge of the nanotube (n,m) index provides us with an assessment of all the nanotube's properties.[12] The first-order Raman scattering feature, the RBM, also gives us information about carbon nanotube metallicity, whether the nanotube is semiconducting (S) or metallic (M). From this, it follows that a DWNT, a system of two concentric nanotubes, can have four different flavors: S@S, M@M, S@M, and M@S (innermost@host tubes). Moreover, the nanotube surroundings can either weakly or strongly interact with the radial vibration of the carbon atoms, and the effects of these interactions are usually manifested as a shift of the ω_{RBM} as well as a change in the full width at half-maximum (fwhm) intensity of the RBM Raman feature. Some environmental interactions, for example, can be introduced by liquids,[13] external pressure/strain,[14] temperature,[13] other carbon nanotubes,[15] substrates on which the nanotubes are sitting,[16] freely suspended nanotubes,[17] or the situation where another concentric nanotube exists either inside or outside within the multiwalled carbon nanotube (MWNT) system.[18]

Recently, on the basis of experimental results obtained for the so-called supergrowth SWNTs,[19] Araujo *et al.* proposed a relation between ω_{RBM} and d_t given by

$$\omega_{RBM} = \frac{227}{d_t}\sqrt{(1 + C_e \cdot d_t^2)} \quad (1)$$

in which $d_t = 0.1421((3(n^2 + nm + m^2))^{1/2})/\pi$ and C_e is the only adjustable parameter to be determined by a fitting procedure.[20] As a matter of fact, C_e is related to the strength of the environmental interactions. The term $C_e \cdot d_t^2$ will be responsible for the changes in ω_{RBM} provided by any environmental interactions between a nanotube with its surroundings. If changes due to the nanotube surroundings are not present, the constant C_e is expected to be zero and the resulting equation

$$\omega_0 = \frac{227}{d_t} \quad (2)$$

should be applied for a nanotube. The constant 227 cm^{-1} nm, which is completely determined by the intrinsic (Young modulus, Poisson ratio, and mass density) properties of the nanotubes, is in accordance with theoretical predictions using the sound velocity of graphite as a parameter in the calculations.[21]

The scientific community is especially interested in the nature of the ω_{RBM} *versus* d_t relation for the innermost tubes in MWNT systems since, by means of departures from the pristine-like relation given by eq 2, it is possible to make important statements about growth methods, shielding effects, strain effects, intertube interaction properties, and their relation with the wall-to-wall (WtW) distances of MWNT systems. In the present work, we address some answers to the effect of these factors by first studying bundled DWNTs and TWNTs which are prepared using various annealing temperatures of the innermost fullerene-peapod-derived tubes, and finally, we discuss individual species to complete the big MWNT picture in more depth. Note that the knowledge of how the properties of the constituent tubes in a MWNT system are changed due to a controlled growth process and therefore changing their environment is fundamental for further technological applications of these nanoscaled materials. In addition, the innermost peapod-derived tubes are good candidates to study tubes with diameters smaller than 1 nm (which implies the presence of curvature-dependent effects in nanotube properties) in an environment expected to be free of any external interactions and an environment that is to first-order only influenced by the concentric first-outer-neighbor (host) tube.

Our recent Raman study of bundled TWNTs, including published ω_{RBM} values from bundled DWNTs, showed that especially the fullerene-peapod-derived innermost tubes have metallicity-dependent C_e constants, where the constant related to semiconducting tubes is larger than that related to metallic tubes.[22] Moreover, it has been shown that the variation of the WtW distance (ΔR_{WtW}) in DWNTs is the reason for the appearance of clusters of peaks in the ω_{RBM} spectrum for many DWNTs with semiconducting innermost tubes.[18] These clusters of peaks that are observed represent characteristic intertube interactions due to ΔR_{WtW} variations.[18,23−26] Our present study aims to differentiate between the resonant RBM characteristics of semiconducting and metallic innermost tubes at a fundamental level. Also, we analyze the relation between the ΔR_{WtW} and the resulting ω_{RBM} upshifts of the innermost tubes in individual fullerene-peapod-derived DWNTs and TWNTs as well as individual CVD DWNTs, which is helpful to better understand the observed RBM trends observed in the Raman spectra for bundled DWNTs and TWNTs.

RESULTS AND DISCUSSION

First, we present detailed RRS results for bundled DWNTs and TWNTs, where in both cases the innermost tubes are prepared by encapsulating fullerene peapods through a high-temperature treatment in an argon atmosphere.[3,10] We gained information about this high-temperature treatment process by studying the effect of the heat treatment between 1500 and 2000 °C at a constant annealing time of 30 min. This helps us to find the optimal growth conditions and to study and evaluate the growth method of the innermost tubes. In Figure 1, high-resolution transmission

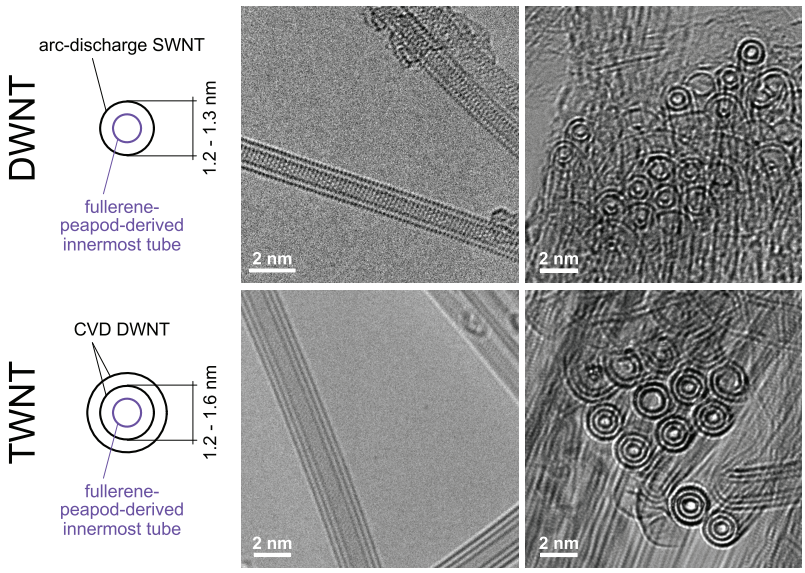

Figure 1. Schematic cross sectional views include the fabrication details for the fullerene-peapod-derived DWNTs and TWNTs. The innermost tubes were produced through a thermal treatment of fullerenes inside of arc-discharge-grown SWNTs and of diameter-enlarged CVD-grown DWNTs.[3,10] The upper (lower) high-resolution TEM images show fullerene-peapod-derived DWNTs (TWNTs).

electron microscopy (TEM) images of DWNTs and TWNTs used in this work can be seen together with the nanotube fabrication details. In order to better distinguish among the RBM features, all the Raman spectra of the bundled nanotube samples were normalized to the strongest RBM peak in the low-frequency range.

The (*n*,*m*) assignments to the observed nanotubes are made based on Kataura's plot, which was adapted from our RBM study on bundled TWNTs,[22] as depicted in Figure 2a. As a reminder, the Kataura plot is a theoretical plot which relates the nanotubes transition energies (E_T) as a function of either the nanotubes' diameters or the nanotubes' RBM frequencies. As a reference, the E_{laser} of 2.41 eV is represented by the solid gray line. Only the carbon nanotube species whose transition energies are in resonance with (or close to) E_{laser} are expected to have their RBMs appearing in the Raman spectrum. It is worth mentioning that our choice for the 2.41 eV laser energy reflects the following facts: this laser line (1) is an ideal laser line to observe RBM features for both metallic and semiconducting innermost tubes in a single spectrum and (2) is a laser line commonly found in laboratories worldwide. With the help of extensive literature on (*n*,*m*) assignments to carbon nanotubes,[20,27−29] we use our experimental Raman spectra to obtain pairs of (E_{laser}, ω_{RBM}) which are compared to the pairs (E_T, ω_{RBM}^{theo}) provided by the theoretical Kataura plot. We then find the (*n*,*m*) indices correlated to each (E_{laser}, ω_{RBM}) pair. Figure 2a shows the possible resonant (*n*,*m*) tubes (organized by families, where $2n + m$ = constant) from the metallic families M14, M18, M21, and M24 (represented by the blue symbols) as well as for the semiconducting families S15, S17, and S20 (red symbols). The green vertical lines correspond to the ω_0 values of the resonant (*n*,*m*) tubes according to eq 2. Later, in the present work, we will see that the RBM intensities around 380 cm^{-1} come from a semiconducting tube (details are shown in Figure 5), so that the only possible species for this frequency region is the (5,4) tube. Also verified by an individual TWNT are the RBM intensities around 324 cm^{-1}, which belong to the metallic (9,0) tube.

Two examples of RBM Raman spectra are shown for the semiconducting innermost fullerene-peapod-derived (5,4) tubes for bundled DWNTs in Figure 2b and for bundled TWNTs in Figure 2c. Using several other E_{laser} excitation energies, we recognized that, for our batch of fabricated DWNT and TWNT samples, the (5,4) tube represents our smallest diameter peapod-grown innermost tube with d_t = 0.61 nm. The RBM spectra of the innermost (5,4) tubes from both the bundled DWNTs and the bundled TWNTs exhibit more peaks for the same innermost tube based on what is known for a SWNT because of a ΔR_{WtW} variation between the innermost tube and host tube. All peaks shown in Figure 2b,c have a fwhm for the Raman intensity of 3 cm^{-1}, while the strongest peak intensity is located at 383.8 cm^{-1}. It is worth commenting that in this work none of the fitting parameters, such as intensity, fwhm intensity, and frequency, was shared during the fitting procedure. These narrow linewidths indicate that the phonon lifetimes are long and the DWNTs and TWNTs are of high nanotube quality. The green solid vertical line at 371.0 cm^{-1} in Figure 2b,c marks the theoretical ω_0 value for the (5,4) tube for which no significant environmental influences are taking place. The larger the upshift of the peak frequency in relation to the green line, the smaller the ΔR_{WtW} to the host tube,

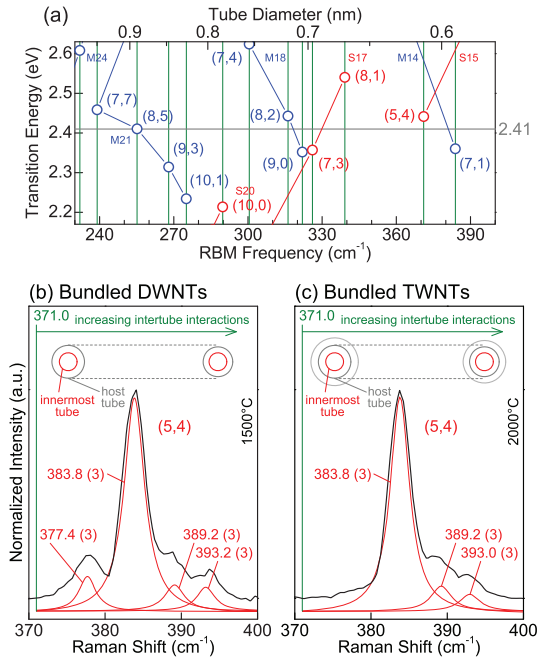

Figure 2. (a) Kataura plot shows the calculated transition energies *vs* the RBM frequency and tube diameter for the expected resonant innermost (*n*,*m*) tubes. The green vertical lines depict the calculated ω_0 values for the presented (*n*,*m*) tubes according to eq 2. Two Raman spectra of the innermost fullerene-peapod-derived (5,4) tubes of bundled (b) DWNTs and (c) TWNTs were taken at E_{laser} = 2.41 eV. The annealing temperatures of the bundled DWNTs (TWNTs) were 1500 °C (2000 °C). These spectra are distinguished by a cluster of peaks for the RBM of one distinct innermost (5,4) tube as a result of the different WtW distances to the host tubes.

which increases the intertube interaction (the green arrows serve as a guide for the eyes). The observed RBM intensities for a semiconducting (5,4) tube in Figure 2b,c make it clear that all RBM values are upshifted in comparison to the expected RBM intensity regarding eq 2. Arvanitidis *et al.* applied various high hydrostatic pressures to DWNTs and studied their Raman spectra with the result that the ω_{RBM} from the innermost tubes upshifts because of a reduction of the ΔR_{WtW} between the two concentric tubes by increasing the pressure.[30−32] Moreover, Pfeiffer *et al.* showed that, for an annealing temperature of 1250 °C, the innermost fullerene-peapod-derived (6,4) tubes grow faster in host tubes with larger diameters.[33] The Raman intensity profiles of both (5,4) clusters in Figure 2b,c are quite similar, but we will show that they have different dependencies on the annealing temperatures. The following Raman studies allow us to make further general statements about intertube interactions in DWNT and TWNT systems.

We plot in Figure 3 the observed resonant RBMs of the innermost tubes in **bundled DWNTs** annealed at different temperatures from 1500 to 1800 °C. At this point, it is important to remember that the starting host SWNT produced by the arc-discharge method was the same for all fullerene-peapod-derived DWNTs reported in the present study. Following the changes of the RBM intensities based on various annealing temperatures and with the help of the Kataura plot shown in Figure 2a, we are able to assign the resonant RBMs and accurately fit the particular (*n*,*m*) tubes with Lorentzian curves. Thereby, we notice various spectral differences in Figure 3 between semiconducting tubes (highlighted as red Lorentzian peaks and red symbols) and metallic tubes (blue Lorentzian peaks and blue symbols).

In detail, the semiconducting innermost tubes in Figure 3 show clusters of narrow peaks with fwhm intensity values between 2.2 and 3.4 cm^{-1}. We observe that these clusters can have their peak positions upshifted by up to 22.2 cm^{-1} from the ω_0 value obtained from eq 2. The narrow peaks are separated between 3.5 and 6.4 cm^{-1}. By changing the annealing temperature in steps of 100 °C between 1500 and 1800 °C, we observed three similar behaviors of the semiconducting (7,3) and (5,4) clusters:

- First, the peaks of the clusters show stronger or weaker intensities depending on their annealing temperatures, but the frequencies of these peaks are not influenced by the annealing temperature.
- Second, the intensity distribution of these two clusters moves toward lower ω_{RBM} values by increasing the annealing temperature. This consequently indicates larger WtW distances between the host and innermost tubes as well as weaker intertube interactions. For example, the cluster of peaks for the (5,4) tube shows a frequency difference of 19.4 cm^{-1} between the peak at 393.2 cm^{-1} at 1500 °C (see also Figure 2b) and the peak developed at 373.8 cm^{-1} obtained by changing the annealing temperature of the peapods to 1800 °C. Pfeiffer *et al.* reported that the cluster of peaks for the semiconducting (6,4) tube consists of up to 10 clearly distinct peaks over a range of 28.9 cm^{-1} (these peaks are separated between 0.8 and 7.6 cm^{-1}).[24,34]
- Third, all clusters are clearly upshifted in relation to the proposed ω_0 values.

In contrast, the metallic innermost tubes in Figure 3 are observed not to split into clusters, and the peaks show fwhm intensities between 6.0 and 10.4 cm^{-1}, which are much larger fwhm values in comparison to the peaks from the semiconducting tubes. Additional spectra taken at 2.41 eV of the metallic family M21 but with higher resolution and at lower temperature show the same characteristics.[35] By changing the annealing temperature, we observe meaningful variations in peak intensities, widths, and positions of the metallic tubes. First, at an annealing temperature of 1500 °C, the RBM intensities from the family M21 are poorly developed, and in contrast, the (8,2) and (9,0) tubes from the family M18 show strong RBM intensities. This intensity distribution changes by increasing

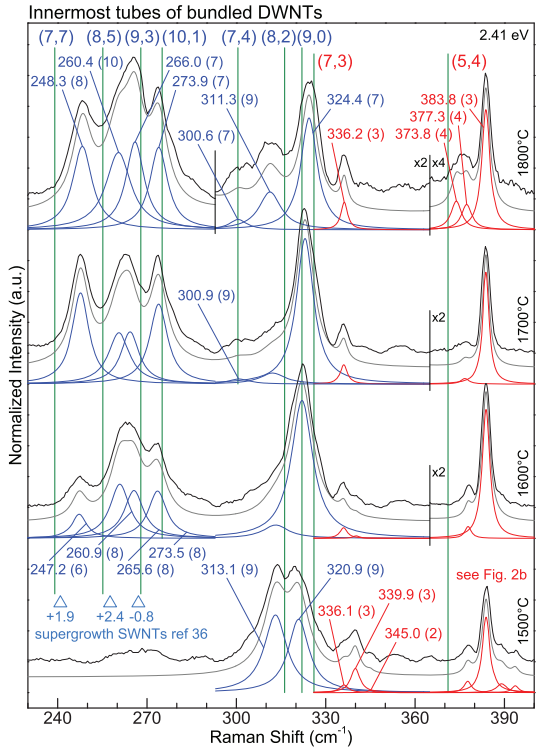

Figure 3. Annealing temperature-dependent spectra taken at E_{laser} = 2.41 eV for the metallic and semiconducting innermost tubes from bundled DWNTs which are annealed between 1500 and 1800 °C. Semiconducting tubes are characterized by clusters of narrow peaks (fitted with red Lorentzian peaks), which are always upshifted in relation to the ω_0 values defined by eq 2. The peak intensity distribution of these clusters shifts toward lower frequencies with increasing annealing temperatures. In contrast, the metallic tubes are distinguished by broader peaks (fitted with blue Lorentzian peaks), and the peak positions of the metallic tubes are located close to the ω_0 values. The spectra show that a high annealing temperature produces larger innermost tube diameters with weaker intertube interactions in comparison to low annealing temperatures. Additionally, we included the experimental ω_{RBM} values (blue triangle symbols) from three metallic as-grown supergrowth SWNTs[36] of the family M21.

the annealing temperature, which points out that higher annealing temperatures produce innermost tubes with larger diameters. Second, the RBM peak widths from metallic tubes with diameters smaller 0.85 nm are observed to narrow by increasing the annealing temperature. This is an indication of a reduction of the intertube interactions at higher temperatures, a characteristic also observed for the innermost semiconducting tubes. Third, we also note that by increasing the annealing temperature, the peak center positions of the metallic tubes undergo a marginal shift, which is different relative to the nonvarying frequency of the peak positions from the semiconducting peaks within the clusters. For example, we can see that the center peak position of the metallic (9,0) tube changes from 320.9 to 324.4 cm^{-1}, and the fwhm decreases from 9 to 7 cm^{-1} by increasing the annealing temperature from 1500 to 1800 °C.

Fourth, in the previous paragraph we observed that the clusters of semiconducting tubes are clearly upshifted (up to 22.2 cm^{-1}) in relation to the respective ω_0 values. Now, in the case of the metallic tubes, we realize that the blue Lorentzian peaks are not only broader but also positioned close to the ω_0 values. At this point, it is worth mentioning that the relation $\omega_0 = 227/d_t$ is used for guidance in comparing the experimental ω_{RBM} between semiconducting and metallic innermost tubes as well as in comparing our observed RBM frequencies with results from other publications. In addition, the ω_0 relation helps to get a better understanding about the fundamental tube properties and the synthesis method used. We also included in Figure 3 the experimental ω_{RBM} values from the (7,7), (8,5), and (9,3) metallic as-grown supergrowth SWNTs[36] using blue triangle symbols, and we also added the frequency difference between the experimental ω_{RBM} value and the ω_0 values. Interestingly, the as-grown supergrowth SWNTs and the innermost tubes from the fullerene-peapod-derived DWNTs show in fact a similar behavior of an upshift as well as a downshift from the ω_0 values. These variations indicate the presence of chirality-dependent interactions along with the metallicity dependence. Moreover, the observed RBM intensity peaks which are downshifted from the ω_0 values can be assumed to correspond to more isolated nanotubes compared to those nanotubes with RBM peak intensities occurring at frequencies above the ω_0 values, but such nanotubes are not completely free from interaction influences, either.

All together, the spectral information obtained from the peak positions, peak widths, and peak intensities allows us to infer that metallic innermost tubes likely exhibit three fundamental behaviors:

- First, the RBM intensities of metallic innermost tubes are not characterized by clusters of narrow, peaks but instead we observe broad individual peaks.
- Second, the center peak positions from these peaks undergo a marginal frequency shift, and the peak widths slightly change by changing the annealing temperature. This could be explained by an overlap of closely located ω_{RBM} values, within the broader linewidth for metallic tubes.
- Third, metallic innermost tubes tend to be more isolated from their adjacent concentric nanotubes, in comparison to semiconducting tubes, as suggested by their ω_{RBM} values being nearby their ω_0 values.

We next discuss the corresponding annealing temperature dependence of the innermost tubes of the **bundled TWNTs,** shown in Figure 4. Here we assigned the RBMs to the metallic (9,0) tube with a broad fwhm intensity and the semiconducting (5,4) tube with a well-structured cluster of narrow peaks, which were

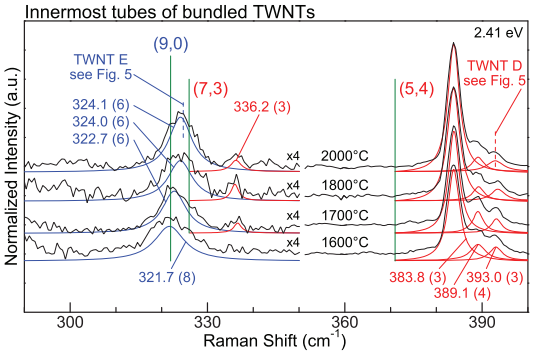

Figure 4. Spectra taken with 2.41 eV for bundled TWNTs fabricated by annealing fullerenes between 1600 and 2000 °C are shown. Under these annealing temperatures, just a few spectral changes are noticed. The two dashed vertical lines (one blue (metallic) and one red (semiconducting)) for the spectrum at 2000 °C represent the ω_{RBM} values of the innermost tubes from two individual TWNTs. The spectral information about these two individual TWNTs can be seen in Figure 5.

clearly distinguishable from the other species in the bundles. In addition, at around 336 cm^{-1}, we notice a very weak RBM intensity for the semiconducting (7,3) tube. In comparison to the spectra for the bundled DWNTs, we see that the resonant intensity profile is weaker for the RBMs of the innermost tubes in the case of the TWNTs. We clearly observe that, by using annealing temperatures between 1600 and 2000 °C, the Raman signals from the innermost tubes for the TWNTs in Figure 4 are not changing as much in intensity and in peak position, in comparison to the corresponding data for the DWNTs in Figure 3 for the innermost tubes. Interestingly, the innermost zigzag (9,0) tube of bundled DWNTs in Figure 3 and of bundled TWNTs in Figure 4 shows an opposite peak position evolution: a small frequency upshift is observed for this metallic tube by increasing the annealing temperatures. Because we expect a decrease of the intertube interactions by going to higher annealing temperature, this upshifting behavior could be as a consequence of either a chirality-dependent intertube interaction or an additional geometrical effect occurring in zigzag tubes. We also observe that our peapod growth method for TWNTs is not as thermally sensitive as for DWNTs because the RBM intensities for the innermost tubes of TWNTs are less affected overall than for DWNTs by using annealing temperatures between 1600 and 2000 °C.

All of the RBM properties of semiconducting and metallic innermost tubes of the bundled DWNTs and TWNTs that are presented above indicate diameter-, metallicity-, and chirality-dependent intertube interactions in fullerene-peapod-derived DWNT and TWNT systems. In the following, we present the results of **individual species** to study the intertube interaction effects in more detail.

The individual TWNTs were identified and characterized with various laser lines utilizing a substrate with fiducial marks, containing patterns that were made by means of e-beam lithography with a subsequent evaporation of a gold grid on top of the Si substrate.[22,37] These fiducial marks help to locate individual tubes in the sample and allow us to measure the same individual nanotube repeatedly.

The low-frequency range in Figure 5 shows the RBMs for the inner and host tubes from five individual TWNTs. Atomic force microscopy (AFM) measurements confirmed that these five individual TWNTs are well-separated from other species on the Si substrate as well as showing that the AFM heights of these TWNT species reflect that their outer tube diameters are around 1.95 ± 0.10 nm.[22] The ω_{RBM} values of outer tubes with such diameters are expected to be around 130 cm^{-1}, which is outside of our detectable spectral range. The upper two spectra belong to two individual TWNTs with semiconducting innermost (6,5) tubes and metallic host tubes. These two inner tubes can be quantitatively compared with published RRS results for 11 individual DWNTs produced at 1700 °C with the same (6,5)@M flavor (innermost@host tube).[26] The S@S flavor for the two inner tubes is represented by the individual TWNT C and TWNT D with the innermost (6,4) and (5,4) tubes. The ω_{RBM} value at 392.9 cm^{-1} from the TWNT D, which is 21.9 cm^{-1} upshifted relative to its ω_0 = 371.0 cm^{-1} value, for the innermost tube of the individual TWNT is assigned to the (5,4) tube with the geometrical calculated diameter of 0.612 nm. This ω_{RBM} value is within the accuracy of the highest identified upshifted RBM peak at 393.0 cm^{-1} in the (5,4) cluster that is observed for the bundled TWNT at 2000 °C shown in Figure 4. This indicates that the intertube interaction is strong for this innermost (5,4) tube when compared to the observation of the (5,4) bundled counterpart in Figure 4. The bottom spectrum in Figure 5 shows a M@S flavor. Here, the (9,0) metallic innermost ω_{RBM} value at 324.7 cm^{-1} agrees well with the fitted Lorentzian peak at 324.1 cm^{-1} of the bundled TWNT at 2000 °C depicted in Figure 4. The innermost (9,0) tube from the TWNT E is a good example of a tube grown in an almost perfectly shielded environment since the RBM upshift is only a 2.8 cm^{-1} upshift in comparison to the ω_0 value given by eq 2.

With regard to the higher spectral range on the right side of Figure 5, a high degree of crystallinity of the TWNTs is concluded given the absence of a significant D-band intensity. We also observed here that the D-band reflects neither a strong nor a very clear dependency on the intertube interaction, which could be understood by considering the symmetry of the vibration of the phonon related to the D-band. The D-band is assigned as the in-plane tangential optical (iTO) mode around the K-point in the Brillouin zone, and its vibration corresponds to an in-plane breathing of the hexagons composing the nanotube lattice. Since

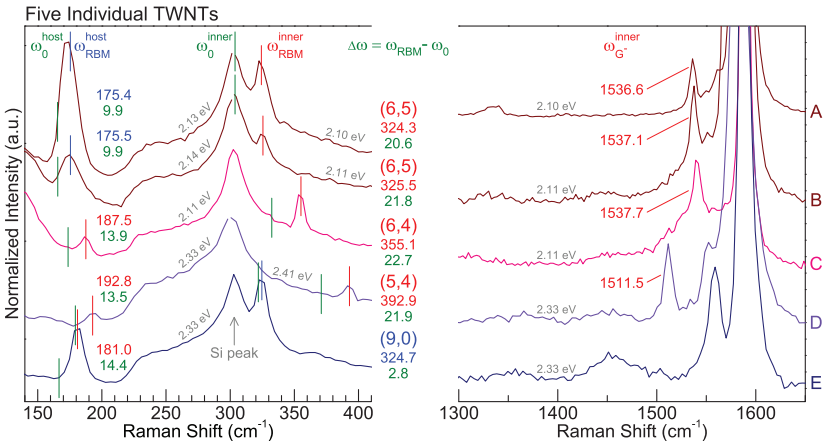

Figure 5. Spectra show the RBM frequency range (left), together with the D-band as well as the G⁻-band frequency range (right) of five individual TWNTs. In the low-frequency range, we see the RBMs from the innermost and host tubes, exhibiting three of the four possible flavors, namely, S@M, S@S, and M@S (innermost@host tubes). The green printed values represent the RBM frequency upshift ($\Delta\omega$) values of the innermost as well as host tubes in relation to the expected $\omega_0 = 227/d_t$ values. The high-frequency range shows the absence of significant D-band intensities and narrow G⁻-bands from the semiconducting innermost tubes. The two bottom spectra represent the two individual TWNTs with an innermost semiconducting (5,4) tube (called TWNT D) and an innermost metallic (9,0) tube (called TWNT E). The ω_{RBM} values of these innermost tubes can be compared with the RBM frequencies observed for the bundled TWNTs at 2000 °C shown in Figure 4.

most force components related to the environmental interactions will be normal to the tube's wall, it is expected that this in-plane mode should not change much when under the effect of such interplanar interactions (note that, in order to see a significant change in the D-band, the environment would need to provide shear force components). However, the iTO mode around the Γ-point, that is manifested in the G⁻-band, is more affected by intertube interaction differences.[26] The iTO modes of SWNTs are diameter-dependent since they are vibrations along the nanotube circumference, and the semiconducting tubes show a narrower G⁻ peak than do the metallic tubes. We observe in Figure 5 for all semiconducting innermost tubes sharp G⁻ peaks, and especially, the G⁻ peak at 1511.5 cm^{-1} of the innermost (5,4) tube is helpful for making accurate statements about the (*n*,*m*) assignments.

Figure 6 represents the experimental ω_{G^-} values as a function of the tube diameters for two individual semiconducting SWNTs[38] as well as for the semiconducting innermost tubes of 11 individual DWNTs[26] and four individual TWNTs. We also included the recently published[38] (magenta solid curve) and the traditional[39] (magenta dashed curve) G⁻ relation for individual semiconducting SWNTs. Telg *et al.* recently reported that the smaller the nanotube diameter, the larger the separation between the experimentally observed G⁻ peak and the calculated G⁻ peak frequency based on its dependence on both family index ($\nu = (n - m)$ mod 3) as well as on chiral angle, whereby nanotubes with $\nu = -1$ show an upshift in frequency and those with $\nu = +1$ show a downshift in frequency in relation to the magenta solid line curve.[38] In Figure 6, we elucidate these observed frequency shifts from the

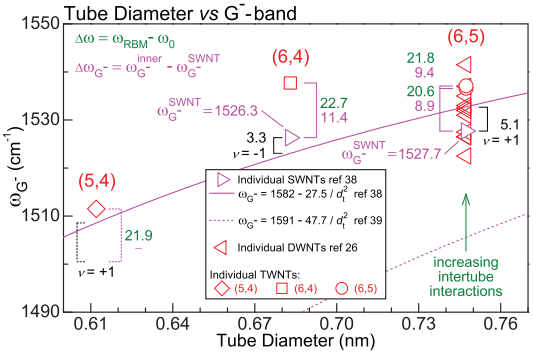

Figure 6. Data shown depict the relation between the experimental ω_{G^-} values of the semiconducting innermost tubes and the respective tube diameters of individual DWNTs[26] and TWNTs. In addition, we plotted the observed ω_{G^-} values of individual (6,4) and (6,5) SWNTs[38] together with two d_t *vs* ω_{G^-} relations for semiconducting SWNTs.[38,39]

SWNTs (black printed values) together with the RBM frequency upshifts ($\Delta\omega$, green printed values) and the G⁻ peak upshifts ($\Delta\omega_{G^-}$, magenta printed values) of the semiconducting innermost tubes from the individual TWNTs. Here, due to a strong intertube interaction, the $\Delta\omega_{G^-}$ values of the TWNTs and most of the DWNTs are upshifted as compared to the ω_{G^-} values for the SWNTs. Moreover, if we take the intertube interaction upshifts into consideration, the ω_{G^-} values of the TWNTs agree well with the ν-dependent behavior, as described from ref 38.

Finally, to better understand the relation between the RBM frequency upshift ($\Delta\omega$) and the WtW distance (ΔR_{WtW}), we merge our experimental findings together with a theoretical model which is presented in ref 18. Several theoretical models have been applied to describe the environmental effects in carbon nanotube

systems by modeling the nanotube as a hollow cylinder. Such models include nanotube interaction with a constant external pressure,[20] in fluids,[40−42] in bundles of nanotubes,[43] and within concentric nanotubes.[44−46] The RBMs for MWNTs can be modeled considering van der Waals' interactions between the nanotubes, either with an atomistic[46] or a continuum[18,44,46] description, resulting in a system of coupled equations for the radial displacements of each nanotube. Given the weak nature of the van der Waals' interaction when compared with the C−C bond, intertube interactions act as a perturbation that modifies the characteristic ω_{RBM} of the RBMs by a few tens of wavenumbers. In the following, we fit the experimental data for the individual DWNTs and TWNTs with the function

$$\frac{\Delta\omega}{\omega_0} = \frac{\omega_{RBM} - \omega_0}{\omega_0} = \left(\frac{A}{\Delta R_{WtW}}\right)^B \quad (3)$$

obtained from the theoretical model in ref 18, where A and B are the fitting parameters. These constants are a measure of the relative change of the intertube forces per unit change of ΔR_{WtW}, with respect to the in-plane forces involved in the breathing mode. In the limit of a large ΔR_{WtW} between the innermost tube and the host tube, the fitting function returns the expected ω_{RBM} of a nanotube with $\omega_0 = 227/d_t$. With this empirical equation, we are able to compare the intertube interaction effects between different MWNT systems.

In order to understand the intertube interactions in MWNT systems, we scrutinized the differences and similarities between individual fullerene-peapod-derived DWNTs and TWNTs as well as individual CVD DWNTs, by utilizing the experimental ω_{RBM} values measured in this work and available in the literature.[25,26,47,48] On one hand, we used the (n,m)-dependent $d_t = 0.1421((3(n^2 + nm + m^2))^{1/2})/\pi$ relation to directly get the tube diameters of the fullerene-peapod-derived innermost tubes and both concentric tubes from the CVD DWNTs. On the other hand, we determined the semiconducting and metallic host tube diameters from the fullerene-peapod-derived species by using eq 1 with $C_e^{S(host)} = 0.097$ nm^{-1} and $C_e^{M(host)} = 0.065$ nm^{-1} from ref 22. These two relations are adapted from a detailed study of the RBMs from bundled TWNTs by using 49 laser excitation energies in the range from 1.55 to 2.54 eV.[22] Interaction effects, as for example the host−outer tube interactions, are already considered in the respective C_e values, allowing us to more accurately and consistently determine the host tube diameters. Interestingly, the $C_e^{M(host)}$ relation for the metallic host tubes is in good agreement with the relation $\omega_{RBM} = 218.3/d_t + 15.9$ cm^{-1} from ref 49, which is the same relation utilized by Villalpando-Paez *et al.* to calculate the host tube diameters from the individual fullerene-peapod-derived DWNTs.[25,26] With the values found for the innermost and host tube diameters, we are able to determine the appropriate WtW distances. More details about the diameter determination as well as the $\Delta\omega$ values of the individual species can be found in the Supporting Information. Next, we plot the ΔR_{WtW} values *versus* the experimental $\Delta\omega$ values for the individual DWNTs[25,26,47,48] in Figure 7a and for the individual TWNTs in Figure 7c.

In Figure 7a, we fit the 13 individual fullerene-peapod-derived and the 14 individual CVD DWNTs with eq 3, and we obtain the values $A = 0.495$ nm and $B = 5.35$ (orange curve) and $A = 0.568$ nm and $B = 5.85$ (red curve), respectively. First of all, we compare the fit relation of individual fullerene-peapod-derived DWNTs with the fit relations for bundled fullerene-peapod-derived DWNTs,[18,50] and we clearly observe that a broader ΔR_{WtW} range of possibilities is expected to exist for $\Delta\omega$ with values of up to 30 cm^{-1} for this growth method. This is mostly reflected by a much lower value of $B = 5.35$ that we found in comparison to the fit relations for bundled fullerene-peapod-derived DWNTs found by Pfeiffer *et al.*,[18,50] where the values for B are 17.22 and 14.2.

Moreover, we observe in Figure 7a that the fit to the individual CVD DWNTs by Liu *et al.*[47] and Levshov *et al.*[48] reveals higher ΔR_{WtW} values when using their $\Delta\omega$ scale compared to the experimental data obtained from fullerene-peapod-derived DWNTs. At this point, it is very important to comment on the fundamental differences between the individual DWNT species measured in these various studies, and indeed, the orange and red curves in Figure 7a reflect the combination of all of these differences: (1) The two concentric tubes by the CVD method grow simultaneously, which also affects the intertube interactions, and of course, the nanotube growth is different when using the peapod growth method, where the innermost tube accommodates the host tube during the growth process. (2) The resulting tube diameters from the fullerene-peapod-derived process produced DWNTs that are considerably smaller than those produced *via* the CVD process. Namely, the innermost fullerene-peapod-derived tubes all have the same diameter $d_{(6,5)} = d_{(9,1)} = 0.747$ nm ($\Delta\omega_{RBM}^{inner} = 18.4$ cm^{-1}), while the CVD-grown innermost tube diameters are between 1.366 and 2.463 nm ($\Delta d_t^{inner} = 1.097$ nm and $\Delta\omega_{RBM}^{inner} = 74$ cm^{-1}). Figure 7b shows the WtW distances *versus* tube diameters of the 14 individual CVD DWNTs from refs 47 and 48. Note that the WtW distance depends on the tube diameters (red dashed lines represent the linear fits), and this diameter-dependent intertube interaction property has to be considered by including the ΔR_{WtW} and $\Delta\omega$ values from the CVD DWNTs in Figure 7a. Furthermore, we know from various publications[18,23,25,34,50] that the formation of clusters of RBM peaks of small innermost (n,m) tube diameters (for example, fullerene- or ferrocene-peapod-derived tubes) is observed due to the few possible

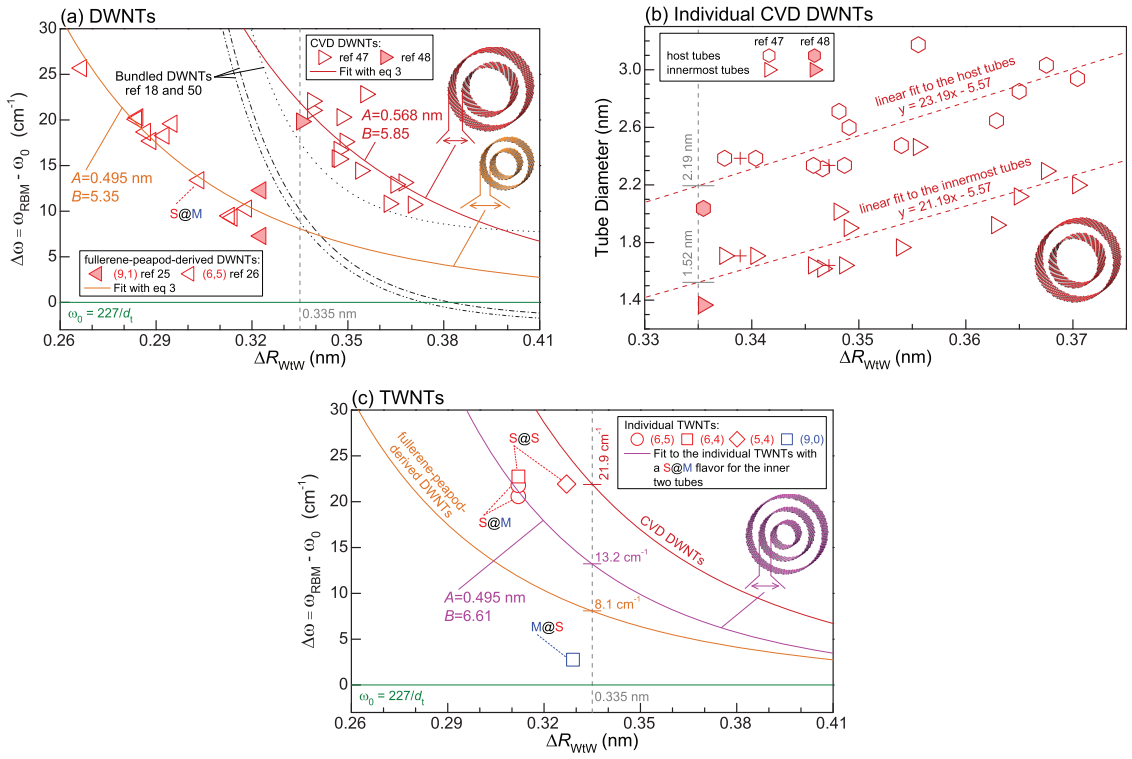

Figure 7. Experimental $\Delta\omega$ values of the innermost tubes are plotted as a function of the experimentally determined WtW distance (ΔR_{WtW}) between the innermost and the host tubes of (a) individual fullerene-peapod-derived[25,26] and CVD[47,48] DWNTs as well as (c) individual fullerene-peapod-derived TWNTs. The orange and purple curves in (a) and (c) represent the fits to the experimental data points with semiconducting innermost and metallic host tubes from both the individual fullerene-peapod-derived DWNTs and the TWNTs by using eq 3. The red curve in (a) and (c) depicts the fit to the 14 individual CVD DWNTs. Also included in panel (a) are fit relations from the literature for RRS studies on bundled fullerene-peapod-derived DWNTs.[18,50] We plotted in panel (b) the ΔR_{WtW} (*x*-axis) *vs* the innermost and host tube diameters (*y*-axis) from the individual CVD DWNTs published by Liu *et al.*[47] and Levshov *et al.*[48] In this plot, we observe diameter-dependent intertube interactions in these individual CVD DWNTs with relatively large diameters in comparison to the fullerene-peapod-derived DWNTs. Throughout the text, we discuss in detail the intertube interaction effects between the two growth methods, with regards to the dependence of the ΔR_{WtW} on the number of concentric tubes as well as on the different flavors of the individual TWNTs. All the presented data points are listed in Table S1 in the Supporting Information.

(*n*,*m*) indices for small diameter tubes at higher ω_{RBM} values. In contrast, the relatively large innermost tube diameters of the CVD DWNTs have many more (*n*,*m*) index possibilities in the same ω_{RBM} region. (3) It is also important to take in account that the measurement strategies are different as the fullerene-peapod-derived species are laying on a Si substrate, while the CVD DWNTs are suspended.

In Figure 7c, we plot the results for the five individual fullerene-peapod-derived TWNTs, with three flavors (S@M, S@S, and M@S) for the two inner tubes. The observation makes clear that the semiconducting innermost tubes of the individual TWNTs can be found close together, but the ΔR_{WtW} values are obviously larger as compared to the fullerene-peapod-derived DWNTs and smaller in comparison to the CVD DWNTs. We focused at first on the data points of the individual DWNTs and TWNTs fabricated with same growth method, characterized with the same Raman setup, with the same S@M flavor for the innermost and host tubes, and with exactly the same innermost tube diameter (0.747 nm). Namely, the 13 individual DWNTs with the (6,5)@M and (9,1)@M flavor (orange curve), together with the two individual TWNTs with the (6,5)@M flavor for the inner two tubes. By comparing the intertube interactions between these concentric tubes, we are able to keep the fitting parameter *A* constant using the value 0.495 nm. The difference between two or three concentric tubes is now only reflected by the fitting parameter *B*, and we are able to determine the value *B* to be 6.61 for the two inner tubes of TWNTs. Our study points out that $\Delta\omega$ values are < 8.1 cm^{-1} (13.2 cm^{-1}) in fullerene-peapod-derived DWNTs (TWNTs) with semiconducting innermost and metallic host tubes that have ΔR_{WtW} values that are larger than the 0.335 nm interlayer distance of graphite.[51]

Next, we can compare the intertube interactions between the three different flavors justified by the fact that the diameters of the fullerene-peapod-derived innermost tubes of the individual TWNTs in Figure 7c are in the same diameter regime with Δd_t^{inner} of only 0.135 nm. First, we observe that the TWNTs with a S@S flavor are upshifted in frequency from the obtained

relation for TWNTs with a S@M flavor, which we attribute to the stronger intertube interactions in a S@S system. In addition, we note that the innermost (5,4) tube also shows flavor-dependent intertube interactions as well as stronger high-curvature interactions which are distinguished by a stronger frequency upshift of the (5,4)@S flavor in comparison to the (6,4)@S flavor. The individual TWNTs containing the metallic innermost (9,0) tube provide a good example of the proposed behavior of bundled DWNTs and TWNTs, where the metallic innermost tubes show less intertube interaction compared to the semiconducting innermost tubes, and as a result, the $\Delta\omega$ value is only 2.8 cm^{-1}. The ΔR_{WtW} between this M@S flavor was calculated to be 0.329 nm, which should be compared to the 0.335 nm value. At this point, we believe that further characterization of individual DWNTs with metallic innermost tubes is required to analyze in greater detail some of the proposed behaviors discussed in this work.

Through the comparison between the three fits (orange, purple, and red curves) shown in Figure 7c, we can make statements with regards to mechanical coupling and interference effects in the multiwalled systems under investigation. Each of the 14 individual CVD DWNTs was reported to show a mechanical coupling mediated by van der Waals' interactions between the two concentric tubes.[47,48] This coupling is reflected by the presence of both RBM peaks from the innermost and host tubes in a single spectrum. Liu *et al.* discussed the observed coupled RBMs using the ansatz of a quantized coupled mechanical oscillator.[47] In their model, strongly coupled oscillations have higher RBM frequencies and both RBMs appear even though only one tube's E_T is in resonance with the utilized E_{laser}. As a matter of fact, the red curve tells us that the intertube interactions in the reported CVD DWNTs[47,48] (A = 0.568 nm and B = 5.85) are stronger in comparison to the fullerene-peapod-derived DWNTs[25,26] as well as to TWNTs. As described above, we are comparing the intertube interactions in two different diameter regions, and it is worth commenting that the number of interacting atoms per unit length scales with the tube diameter. In good agreement in this content are the individual fullerene-peapod-derived DWNTs with the innermost tube diameters of only 0.747 nm (A = 0.495 nm and B = 5.35), which show comparatively weak intertube interactions. Adding to a fullerene-peapod-derived DWNT an additional outer tube (purple curve), our results show that the intertube interactions between the innermost and host tube increases, but that the interactions are not as strong as in the CVD DWNTs. The results discussed in the beginning of this work for the annealing temperature-dependent RBM spectra from the fullerene-peapod-derived bundled DWNTs (Figure 3) and TWNTs (Figure 4) also showed that by increasing the annealing temperature for the DWNTs we can decrease the intertube interactions. Since the TWNTs are thermally more stable, we found that the intertube interaction reduction is not as strong as it is for the annealing temperature-sensitive DWNTs. At this point, it is important to remember that the individual fullerene-peapod-derived DWNTs (TWNTs) were prepared using an annealing temperature of 1700 °C (2000 °C).

Interestingly, our individual TWNTs do not experience mechanical coupling and interference effects between the two inner tubes. This is verified by three experimental observations: First, the centers of the RBM resonant windows from the innermost and host tubes are not positioned at the same E_{laser}. One resonance RBM profile of an individual TWNT, which confirms this, is shown in Figure 5b of our recent publication.[22] Second, through the scanning process of our measurement strategy, we were able to find dozens of other individual TWNTs, but even by using different laser energies, it was not possible to get in resonance simultaneously with more than one RBM of each TWNT. Third, the experimental 2D map representing the RBM intensities of bundled TWNTs[22] as a function of the ω_{RBM} and E_{laser} shows that the RBMs of the innermost and host tubes are in resonance, independent from each other. This observation also can be seen in the 2D intensity maps of bundled fullerene-peapod-derived DWNTs shown in refs 23 and 25.

CONCLUSION

In summary, we reported here RRS studies of individual and bundled DWNTs as well as TWNTs. We observed a number of similarities and differences in the RBMs of the innermost tubes in bundled fullerene-peapod-derived DWNTs and TWNTs. Here, the metallic innermost tubes are distinguished by their broad resonant peaks relative to the clusters of narrow peaks of the semiconducting tubes. In addition, the metallic innermost tubes can be considered to be more isolated from their adjacent concentric nanotubes in comparison to the semiconducting tubes because the metallic RBM frequencies are located nearby to ω_0, while the clusters of peaks for semiconducting innermost tubes are always upshifted in frequency in comparison to ω_0. The peak intensity distributions of the semiconducting innermost tubes in DWNTs shift toward lower ω_{RBM} for higher annealing temperatures, which indicates that higher annealing temperatures tend to reduce the intertube interaction in fullerene-peapod-derived DWNTs generally. The annealing process for the innermost tubes in fullerene-peapod-derived TWNTs is not as temperature-sensitive in comparison to the fullerene-peapod-derived DWNTs, which shows that the innermost tubes in TWNTs are thermally more stable. Depending on the intertube interaction differences between individual fullerene-peapod-derived DWNTs

and TWNTs, the RBMs as well as the iTO modes (G^--band) of the innermost tubes show significant Raman frequency upshifts. An analysis of the RBM frequency upshifts in relation to the WtW distances between the innermost and host tubes from individual fullerene-peapod-derived DWNTs and TWNTs as well as from individual CVD DWNTs helps us to make more precise statements about diameter-, metallicity-, chirality-, flavor-, and high-curvature-dependent intertube interactions in DWNT and TWNT systems.

MATERIALS AND METHODS

The bundled DWNTs (TWNTs) are prepared through high-temperature treatments of the peapod fullerenes inside of arc-discharge-grown SWNTs (diameter-enlarged CVD-grown DWNTs) at temperatures between 1500 and 2000 °C using a graphite furnace in argon.[3,10] The spectra of the bundled samples were taken at room temperature using a Raman setup comprising a triple grating spectrometer (TU München) with a laser energy $E_{laser} = 2.41$ eV. The spectra of the individual species were taken with a home-built single-grating spectrometer (MIT) operated at room temperature, and this Raman setup includes the following lasers: an argon ion laser, a Nd:YAG laser, two tunable dye lasers (DCM and rhodamine dye), and a Ti:sapphire laser.

Conflict of Interest: The authors declare no competing financial interest.

Acknowledgment. We thank J.A. Garrido and F. Herzog (TU München) as well as A. Hartschuh and N. Hartmann (LMU München) for experimental support. P.T.A., J.F.R.-N., and M.S.D. acknowledge the NSF-DMR 10-04147 grant. H.M. acknowledges support from the JSPS KAKENHI Grant Number 24710115. Y.A.K. acknowledges the support from Global Research Laboratory (2013056090) through the National Research Foundation of Korea (NRF) funded by the Ministry of Science, ICT (Information and Communication Technologies) and Future Planning.

Supporting Information Available: We present all experimental and calculated values from the 13 individual fullerene-peapod-derived DWNTs,[25,26] the 14 individual CVD DWNTs,[47,48] and the five individual TWNTs of the present work. This material is available free of charge *via* the Internet at http://pubs.acs.org.

REFERENCES AND NOTES

1. Endo, M.; Muramatsu, H.; Hayashi, T.; Kim, Y. A.; Terrones, M.; Dresselhaus, M. S. Buckypaper from Coaxial Nanotubes. *Nature* **2005**, *433*, 476.
2. Sugai, T.; Yoshida, H.; Shimada, T.; Okazaki, T.; Shinohara, H.; Bandow, S. New Synthesis of High-Quality Double-Walled Carbon Nanotubes by High-Temperature Pulsed Arc Discharge. *Nano Lett.* **2003**, *3*, 769–773.
3. Muramatsu, H.; Hayashi, T.; Kim, Y. A.; Shimamoto, D.; Endo, M.; Meunier, V.; Sumpter, B. G.; Terrones, M.; Dresselhaus, M. S. Bright Photoluminescence from the Inner Tubes of "Peapod"-Derived Double-Walled Carbon Nanotubes. *Small* **2009**, *5*, 2678–2682.
4. Smith, B. W.; Monthioux, M.; Luzzi, D. E. Encapsulated C_{60} in Carbon Nanotubes. *Nature* **1998**, *396*, 323.
5. Hernandez, E.; Meunier, V.; Smith, B. W.; Rurali, R.; Terrones, H.; Buongiorno Nardelli, M.; Terrones, M.; Luzzi, D. E.; Charlier, J.-C. Fullerene Coalescence in Nanopeapods: A Path to Novel Tubular Carbon. *Nano Lett.* **2003**, *3*, 1037–1042.
6. Bandow, S.; Takizawa, M.; Hirahara, K.; Yudasaka, M.; Iijima, S. Raman Scattering Study of Double-Wall Carbon Nanotubes Derived from the Chains of Fullerenes in Single-Wall Carbon Nanotubes. *Chem. Phys. Lett.* **2001**, *337*, 48–54.
7. Li, Y.; Hatakeyama, R.; Kaneko, T.; Okada, T. Nano Sized Magnetic Particles with Diameters Less than 1 nm Encapsulated in Single-Walled Carbon Nanotubes. *Jpn. J. Appl. Phys.* **2006**, *45*, L428–L431.
8. Kuzmany, H.; Plank, W.; Schaman, C.; Pfeiffer, R.; Hasi, F.; Simon, F.; Rotas, G.; Pagona, G.; Tagmatarchis, N. Raman Scattering from Nanomaterials Encapsulated into Single Wall Carbon Nanotubes. *J. Raman Spectrosc.* **2007**, *38*, 704–713.
9. Chernov, A. I.; Fedotov, P. V.; Talyzin, A. V.; Suarez Lopez, I.; Anoshkin, I. V.; Nasibulin, A. G.; Kauppinen, E. I.; Obraztsova, E. D. Optical Properties of Graphene Nanoribbons Encapsulated in Single-Walled Carbon Nanotubes. *ACS Nano* **2013**, *7*, 6346–6353.
10. Muramatsu, H.; Shimamoto, D.; Hayashi, T.; Kim, Y. A.; Terrones, M.; Endo, M.; Dresselhaus, M. S. Bulk Synthesis of Narrow Diameter and Highly Crystalline Triple-Walled Carbon Nanotubes by Coalescing Fullerene Peapods. *Adv. Mater.* **2011**, *23*, 1761–1764.
11. Jorio, A.; Dresselhaus, M. S.; Saito, R.; Dresselhaus, G. *Raman Spectroscopy in Graphene Related Systems*; Wiley-VCH: Weinheim, Germany, 2011.
12. Dresselhaus, M. S.; Dresselhaus, G.; Saito, R.; Jorio, A. Raman Spectroscopy of Carbon Nanotubes. *Phys. Rep.* **2005**, *409*, 47–99.
13. Fantini, C.; Jorio, A.; Souza, M.; Strano, M. S.; Dresselhaus, M. S.; Pimenta, M. A. Optical Transition Energies for Carbon Nanotubes from Resonant Raman Spectroscopy: Environment and Temperature Effects. *Phys. Rev. Lett.* **2004**, *93*, 147406.
14. Venkateswaran, U. D.; Masica, D. L.; Sumanasekera, G. U.; Furtado, C. A.; Kim, U. J.; Eklund, P. C. Diameter Dependent Wall Deformations during the Compression of a Carbon Nanotube Bundle. *Phys. Rev. B* **2003**, *68*, 241406(R).
15. Rao, A. M.; Chen, J.; Richter, E.; Schlecht, U.; Eklund, P. C.; Haddon, R. C.; Venkateswaran, U. D.; Kwon, Y.-K.; Tomanek, D. Effect of van der Waals Interactions on the Raman Modes in Single Walled Carbon Nanotubes. *Phys. Rev. Lett.* **2001**, *86*, 3895–3898.
16. Jorio, A.; Saito, R.; Hafner, J. H.; Lieber, C. M.; Hunter, M.; McClure, T.; Dresselhaus, G.; Dresselhaus, M. S. Structural (n,m) Determination of Isolated Single-Wall Carbon Nanotubes by Resonant Raman Scattering. *Phys. Rev. Lett.* **2001**, *86*, 1118–1121.
17. Meyer, J. C.; Paillet, M.; Michel, T.; Moreac, A.; Neumann, A.; Duesberg, G. S.; Roth, S.; Sauvajol, J.-L. Raman Modes of Index-Identified Freestanding Single-Walled Carbon Nanotubes. *Phys. Rev. Lett.* **2005**, *95*, 217401.
18. Pfeiffer, R.; Kramberger, C.; Simon, F.; Kuzmany, H.; Popov, V. N.; Kataura, H. Interaction between Concentric Tubes in DWCNTs. *Eur. Phys. J. B* **2004**, *42*, 345–350.
19. Hata, K.; Futaba, D. N.; Mizuno, K.; Namai, T.; Yumura, M.; Iijima, S. Water-Assisted Highly Efficient Synthesis of Impurity-Free Single-Walled Carbon Nanotubes. *Science* **2004**, *306*, 1362–1364.
20. Araujo, P. T.; Maciel, I. O.; Pesce, P. B. C.; Pimenta, M. A.; Doorn, S. K.; Qian, H.; Hartschuh, A.; Steiner, M.; Grigorian, L.; Hata, K.; *et al.* Nature of the Constant Factor in the Relation between Radial Breathing Mode Frequency and Tube Diameter for Single-Wall Carbon Nanotubes. *Phys. Rev. B* **2008**, *77*, 241403 (R).
21. Mahan, G. D. Oscillations of a Thin Hollow Cylinder: Carbon Nanotubes. *Phys. Rev. B* **2002**, *65*, 235402.
22. Hirschmann, T. Ch.; Araujo, P. T.; Muramatsu, H.; Zhang, X.; Nielsch, K.; Kim, Y. A.; Dresselhaus, M. S. Characterization of Bundled and Individual Triple-Walled Carbon Nanotubes by Resonant Raman Spectroscopy. *ACS Nano* **2013**, *7*, 2381–2387.
23. Pfeiffer, R.; Simon, F.; Kuzmany, H.; Popov, V. N. Fine Structure of the Radial Breathing Mode of Double-Wall Carbon Nanotubes. *Phys. Rev. B* **2005**, *72*, 161404(R).
24. Pfeiffer, R.; Simon, F.; Kuzmany, H.; Popov, V. N.; Zolyomi, V.; Kürti, J. Tube−Tube Interaction in Double-Wall Carbon Nanotubes. *Phys. Status Solidi B* **2006**, *243*, 3268–3272.

25. Villalpando-Paez, F.; Moura, L. G.; Fantini, C.; Muramatsu, H.; Hayashi, T.; Kim, Y. A.; Endo, M.; Terrones, M.; Pimenta, M. A.; Dresselhaus, M. S. Tunable Raman Spectroscopy Study of CVD and Peapod-Derived Bundled and Individual Double-Wall Carbon Nanotubes. *Phys. Rev. B* **2010**, *82*, 155416.
26. Villalpando-Paez, F.; Muramatsu, H.; Kim, Y. A.; Farhat, H.; Endo, M.; Terrones, M.; Dresselhaus, M. S. Wall-to-Wall Stress Induced in (6,5) Semiconducting Nanotubes by Encapsulation in Metallic Outer Tubes of Different Diameters: A Resonance Raman Study of Individual C_{60}-Derived Double-Wall Carbon Nanotubes. *Nanoscale* **2010**, *2*, 406–411.
27. Pfeiffer, R. Dispersion of Raman Lines in Carbon Nanophases. Ph.D. Thesis, Universität Wien, 2004; pp 75−76.
28. Araujo, P. T.; Doorn, S. K.; Kilina, S.; Tretiak, S.; Einarsson, E.; Maruyama, S.; Chacham, H.; Pimenta, M. A.; Jorio, A. Third and Fourth Optical Transitions in Semiconducting Carbon Nanotubes. *Phys. Rev. Lett.* **2007**, *98*, 067401.
29. Doorn, S. K.; Araujo, P. T.; Hata, K.; Jorio, A. Excitons and Exciton−Phonon Coupling in Metallic Single-Walled Carbon Nanotubes: Resonance Raman Spectroscopy. *Phys. Rev. B* **2008**, *78*, 165408.
30. Arvanitidis, J.; Christofilos, D.; Papagelis, K.; Andrikopoulos, K. S.; Takenobu, T.; Iwasa, Y.; Kataura, H.; Ves, S.; Kourouklis, G. A. Pressure Screening in the Interior of Primary Shells in Double-Wall Carbon Nanotubes. *Phys. Rev. B* **2005**, *71*, 125404.
31. Arvanitidis, J.; Christofilos, D.; Papagelis, K.; Takenobu, T.; Iwasa, Y.; Kataura, H.; Ves, S.; Kourouklis, G. A. Double-Wall Carbon Nanotubes under Pressure: Probing the Response of Individual Tubes and Their Intratube Correlation. *Phys. Rev. B* **2005**, *72*, 193411.
32. Christofilos, D.; Arvanitidis, J.; Kourouklis, G. A.; Ves, S.; Takenobu, T.; Iwasa, Y.; Kataura, H. Identification of Inner and Outer Shells of Double-Wall Carbon Nanotubes Using High-Pressure Raman Spectroscopy. *Phys. Rev. B* **2007**, *76*, 113402.
33. Pfeiffer, R.; Holzweber, M.; Peterlik, H.; Kuzmany, H.; Liu, Z.; Suenaga, K.; Kataura, H. Dynamics of Carbon Nanotube Growth from Fullerenes. *Nano Lett.* **2007**, *7*, 2428–2434.
34. Shiozawa, H.; Pichler, T.; Grüneis, A.; Pfeiffer, R.; Kuzmany, H.; Liu, Z.; Suenaga, K.; Kataura, H. A Catalytic Reaction Inside a Single-Walled Carbon Nanotube. *Adv. Mater.* **2008**, *20*, 1443–1449.
35. Pfeiffer, R.; Kuzmany, H.; Kramberger, Ch.; Schaman, Ch.; Pichler, T.; Kataura, H.; Achiba, Y.; Kürti, J.; Zolyomi, V. Unusual High Degree of Unpertubed Environment in the Interior of Single-Wall Carbon Nanotubes. *Phys. Rev. Lett.* **2003**, *90*, 225501.
36. Araujo, P. T.; Fantini, C.; Lucchese, M. M.; Dresselhaus, M. S.; Jorio, A. The Effect of Environment on the Radial Breathing Mode of Supergrowth Single Wall Carbon Nanotubes. *Appl. Phys. Lett.* **2009**, *95*, 261902.
37. Villalpando-Paez, F.; Son, H.; Nezich, D.; Hsieh, Y. P.; Kong, J.; Kim, Y. A.; Shimamoto, D.; Muramatsu, H.; Hayashi, T.; Endo, M.; *et al.* Raman Spectroscopy Study of Isolated Double-Walled Carbon Nanotubes with Different Metallic and Semiconducting Configurations. *Nano Lett.* **2008**, *8*, 3879–3886.
38. Telg, H.; Duque, J. G.; Staiger, M.; Tu, X.; Hennrich, F.; Kappes, M. M.; Zheng, M.; Maultzsch, J.; Thomsen, C.; Doorn, S. K. Chiral Index Dependence of the G^+ and G^- Raman Modes in Semiconducting Carbon Nanotubes. *ACS Nano* **2012**, *6*, 904–911.
39. Jorio, A.; Souza Filho, A. G.; Dresselhaus, G.; Dresselhaus, M. S.; Swan, A. K.; Unlü, M. S.; Goldberg, B. B.; Pimenta, M. A.; Hafner, J. H.; Lieber, C. M.; *et al.* G-Band Resonant Raman Study of 62 Isolated Single-Wall Carbon Nanotubes. *Phys. Rev. B* **2002**, *65*, 155412.
40. Longhurst, M. J.; Quirke, N. The Environmental Effect on the Radial Breathing Mode of Carbon Nanotubes in Water. *J. Chem. Phys.* **2006**, *124*, 234708.
41. Longhurst, M. J.; Quirke, N. The Environmental Effect on the Radial Breathing Mode of Carbon Nanotubes. II. Shell Model Approximation for Internally and Externally Adsorbed Fluids. *J. Chem. Phys.* **2006**, *125*, 184705.
42. Longhurst, M. J.; Quirke, N. Pressure Dependence of the Radial Breathing Mode of Carbon Nanotubes: The Effect of Fluid Adsorption. *Phys. Rev. Lett.* **2007**, *98*, 145503.
43. Henrard, L.; Popov, V. N.; Rubio, A. Influence of Packing on the Vibrational Properties of Infinite and Finite Bundles of Carbon Nanotubes. *Phys. Rev. B* **2001**, *64*, 205403.
44. Dobardzic, E.; Maultzsch, J.; Milosevic, I.; Thomsen, C.; Damnjanovic, M. The Radial Breathing Mode Frequency in Double-Walled Carbon Nanotubes: An Analytical Approximation. *Phys. Status Solidi B* **2003**, *237*, R7–R10.
45. Wang, C. Y.; Ru, C. Q.; Mioduchowski, A. Free Vibration of Multiwall Carbon Nanotubes. *J. Chem. Phys.* **2005**, *97*, 114323.
46. Popov, V. N.; Henrard, L. Breathinglike Phonon Modes of Multiwalled Carbon Nanotubes. *Phys. Rev. B* **2002**, *65*, 235415.
47. Liu, K.; Hong, X.; Wu, M.; Xiao, F.; Wang, W.; Bai, X.; Ager, J. W.; Aloni, S.; Zettl, A.; Wang, E.; *et al.* Quantum-Coupled Radial-Breathing Oscillations in Double-Walled Carbon Nanotubes. *Nat. Commun.* **2013**, *4*, 1375.
48. Levshov, D.; Than, T. X.; Arenal, R.; Popov, V. N.; Parret, R.; Paillet, M.; Jourdain, V.; Zahab, A. A.; Michel, T.; Yuzyuk, Yu. I.; *et al.* Experimental Evidence of a Mechanical Coupling between Layers in an Individual Double-Walled Carbon Nanotube. *Nano Lett.* **2011**, *11*, 4800–4804.
49. Endo, M.; Kim, Y. A.; Hayashi, T.; Muramatsu, H.; Terrones, M.; Saito, R.; Villalpando-Paez, F.; Chou, S. G.; Dresselhaus, M. S. Nanotube Coalescence-Inducing Mode: A Novel Vibrational Mode in Carbon Systems. *Small* **2006**, *2*, 1031–1036.
50. Pfeiffer, R.; Peterlik, H.; Kuzmany, H.; Simon, F.; Pressl, K.; Knoll, P.; Rümmeli, M. H.; Shiozawa, H.; Muramatsu, H.; Kim, Y. A.; *et al.* A Detailed Comparison of CVD Grown and Precursor Based DWCNTs. *Phys. Status Solidi B* **2008**, *245*, 1943–1946.
51. Bacon, R. Growth, Structure, and Properties of Graphite Whiskers. *J. Appl. Phys.* **1960**, *31*, 283–290.